*J. Fluid Mech.* (1996), *vol.* 329, *pp.* 373–388



# Laminar flow in rotating curved pipes

By HIROSHI ISHIGAKI

Kakuda Research Center, National Aerospace Laboratory
Kakuda, Miyagi 981-15, Japan

(Received 23 October 1995 and in revised form 21 June 1996)

When a curved pipe rotates about the centre of curvature, the fluid flowing in it is subjected to both Coriolis and centrifugal forces. Based on the analogy between laminar flows in stationary curved pipes and in orthogonally rotating pipes, the flow characteristics of fully developed laminar flow in rotating curved pipes are made clear and definite by similarity arguments, computational studies and using experimental data. Similarity arguments clarify that the flow characteristics in loosely coiled rotating pipes are governed by three parameters: the Dean number $K_{LC}$, a body force ratio $F$ and the Rossby number $Ro$. As the effect of $Ro$ is negligible when $Ro$ is large, computational results are presented for this case first, and then the effect of $Ro$ is studied. Flow structure and friction factor are studied in detail. Variations of flow structure show secondary flow reversal at $F \approx -1$, where the two body forces are of the same order but in opposite directions. It is also shown how the Taylor–Proudman effect dominates the flow structure when $Ro$ is small. Computed curves of the friction factor for constant Dean number have their minimum at $F \approx -1$. A composite parameter $K_L$ is introduced as a convenient governing parameter and used to correlate the characteristics. By applying $K_L$ to the analogy formula previously derived for two limiting flows, a semi-empirical formula for the friction factor is presented, which shows good agreement with the experimental data for a wide range of the parameters.

## 1. Introduction

A quantitative analogy between flows in stationary curved pipes and orthogonally rotating straight pipes has been reported in previous papers (Ishigaki 1994, 1996*a*). Taking this analogy as a basis, this paper describes the characteristics of more general and complicated flow in rotating curved pipes, which are relevant to systems involving helically or spirally coiled pipes rotating about the coil axis. Such rotating flow passages are used in cooling systems in rotating machinery such as gas turbines, electric generators and electric motors. The flow systems are also encountered in separation processes.

When a viscous fluid flows in a coiled pipe rotating at a constant angular velocity about the coil axis, two kinds of secondary flow occur perpendicular to the primary axial flow. One is caused by a centrifugal force due to the curvature of the pipe, the other by a Coriolis force due to the rotation of the pipe. When rotation is in the same direction as the axial flow (positive rotation), the directions of the two secondary flows are the same, and the flow structure remains qualitatively the same as that observed in stationary curved pipes. When rotation is against the axial flow (negative

rotation), the secondary flows are in opposite directions, and particularly complex behaviour can be observed when the magnitudes of the forces are of the same order.

There have been various studies on rotating curved duct flows since the initial work of Ludwieg (1951), who analysed and performed experiments on the flow in a rotating curved duct of square cross-section. Miyazaki (1971, 1973) analysed the laminar boundary layer flow and heat transfer in rotating curved pipes of circular and rectangular cross-sections for the case of positive rotation. Ito & Motai (1974) first analysed the flow in a curved pipe with negative rotation, and showed the reversal of the direction of the secondary flow. These analyses were based on boundary layer approximations.

The flow structure in an inviscid core is so complicated and the interactions with the wall boundary layer are so strong in rotating curved pipe flows that the flow phenomena have to be analysed with the Navier–Stokes equations. In this way, Ito *et al.* (1987, 1988) made finite-difference computations, together with experiments on the friction factor, for the flow in rotating curved pipes for the cases of constant Dean number and of constant rotational Reynolds number. Their computations were, however, limited to relatively small values of the parameters. Computation using orthogonal collocation was done by Daskopoulos & Lenhoff (1990), who paid particular attention to the bifurcation structure of the flow. A bifurcation study was also made by Selmi, Nandakumar & Finlay (1994) for the flow in square ducts. Flow instabilities in rotating curved channels without secondary flow were studied by Matsson & Alfredsson (1990, 1994) and Matsson (1993).

The pressure loss of the flow is the most important subject in engineering. Measurements on the friction factor were conducted by Euteneur & Piesche (1978) and Ito *et al.* (1987, 1988) for circular pipes, and by Ludwieg (1951), Piesche & Felsch (1980), and Piesche (1982) for rectangular ducts. These studies confirmed that the pressure drop is significantly higher than that for non-rotating straight pipes. No experimental data on other flow properties seems to be available.

As the flow is more complex than that with no or one body force, considerations of dynamical similarity are essential as guidance. However, there have been no similarity arguments on the flow in rotating curved pipes. In the above mentioned studies, parameters were adopted quite arbitrarily. Some works used the Reynolds number $Re = w_m d/\nu$ to describe the flow characteristics, where $w_m$ denotes the average flow velocity through the pipe, $d$ the diameter of the pipe and $\nu$ the fluid kinematic viscosity. However, $Re$ includes no effect of curvature or rotation. Ito *et al.* (1987, 1988) used two parameters: the Dean number $K_{LC} = Re/\lambda^{1/2}$ and the rotational Reynolds number $R_\Omega = \Omega d^2/\nu$, where $\lambda = R/d$ is the curvature parameter, $R$ the mean radius of curvature and $\Omega$ the angular velocity of rotation. Daskopoulos & Lenhoff (1990) also used two parameters: the Dean number based on the pressure gradient and a parameter they called the Taylor number $Ta = dR\Omega/(\nu\lambda^{1/2})$. In the dimensionless governing equations of these studies, $\lambda$ oddly appeared as a third parameter in spite of their loose coil assumption. One of the main objectives of this paper is to make the dynamical similarity and governing parameters of the flow clear and definite.

The flow in rotating curved pipes has two limiting situations: flow in a stationary curved pipe without the rotation effect and flow in an orthogonally rotating straight pipe without the curvature effect. The dynamical similarity of steady laminar flow in non-rotating curved pipes depends on the Dean number $K_{LC}$ and the curvature parameter $\lambda$, while that of rotating straight pipe flow depends on a parameter $K_{LR} = Re/|Ro|^{1/2}$ and the Rossby number $Ro = w_m/\Omega d$ (Ishigaki 1994). Accord-

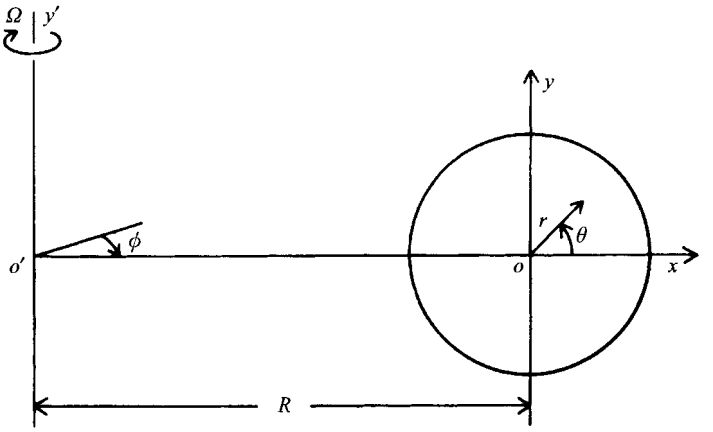


FIGURE 1. Configuration of rotating curved pipe flow.

ingly, the general flow situation in rotating curved pipes will be governed by four parameters: $K_{LC}, \lambda, K_{LR}$ and $Ro$. The beneficial property of the combination of these parameters is that, when $\lambda$ or $Ro$ is large, the flow characteristics are independent of it respectively.

It was revealed in the previous paper (Ishigaki 1994) that, when both of $\lambda$ and $Ro$ are large enough for these effects to be negligible, there is a quantitative analogy between these two limiting flows when $K_{LC} = K_{LR}$. The friction factors of the two flows coincide and flow patterns, as well as flow properties, show strong similarities. Taking this analogy into consideration, analysis will be made first for the case when both $Ro$ and $\lambda$ are large.

When $Ro$ is small in rotating fluid, the Taylor–Proudman effect may generally appear, where fluid motions tend to be invariant along a direction parallel to the rotation axis (Greenspan 1968; Hopfinger 1994). It will be shown how the phenomena affect the flow characteristics in rotating curved pipes.

Two important aspects of the flow will be studied in detail: flow structure and friction factor. Flow structure will be discussed systematically for a wide range of parameters. Computed results of the friction factor will be compared with extensive experimental data by Ito *et al.* (1987, 1988). Through the correlation of friction factor, a convenient governing parameter for the laminar flow in rotating curved pipes will be introduced. A semi-empirical formula for friction factor will be given for large-$Ro$ flow and then this will be extended to include the effect of the Rossby number.

## 2. Governing equations and computational method

The toroidal coordinates $(r, \theta, \phi)$ fixed to a rotating curved pipe are used, as shown in figure 1. The pipe rotates about the $y'$-axis at a constant angular velocity $\Omega$. Positive rotation is when $\Omega > 0$, meaning that the rotation is in the same direction as the main flow in the pipe. Negative rotation is when $\Omega < 0$. The velocities in the directions of $(r, \theta, \phi)$ are denoted by $(u, v, w)$. It is assumed that the flow is incompressible, steady, laminar and fully developed. As the radius of curvature of the curved pipe is much larger than the pipe radius in most of the applications, we introduce a 'loose coil approximation' where $\lambda$ is large enough for the flow properties to be independent of $\lambda$. Rewritten in terms of $z = R\phi$, the equations of continuity

and momentum are as follows:

$$\frac{\partial}{\partial r}(ru) + \frac{\partial v}{\partial \theta} = 0 , \tag{2.1}$$

$$u\frac{\partial u}{\partial r} + \frac{v}{r}\frac{\partial u}{\partial \theta} - \frac{v^2}{r} = -\frac{1}{\rho}\frac{\partial p^*}{\partial r} + \frac{w^2\cos\theta}{R} + 2\Omega w\cos\theta + \nu\left(\nabla^2 u - \frac{u}{r^2} - \frac{2}{r^2}\frac{\partial v}{\partial \theta}\right) , \tag{2.2}$$

$$u\frac{\partial v}{\partial r} + \frac{v}{r}\frac{\partial v}{\partial \theta} + \frac{uv}{r} = -\frac{1}{\rho r}\frac{\partial p^*}{\partial \theta} - \frac{w^2\sin\theta}{R} - 2\Omega w\sin\theta + \nu\left(\nabla^2 v - \frac{v}{r^2} + \frac{2}{r^2}\frac{\partial u}{\partial \theta}\right) , \tag{2.3}$$

$$u\frac{\partial w}{\partial r} + \frac{v}{r}\frac{\partial w}{\partial \theta} = -\frac{1}{\rho}\frac{\partial p^*}{\partial z} - 2\Omega(u\cos\theta - v\sin\theta) + \nu\nabla^2 w , \tag{2.4}$$

where the Laplacian operator is

$$\nabla^2 = \frac{1}{r}\frac{\partial}{\partial r}\left(r\frac{\partial}{\partial r}\right) + \frac{1}{r^2}\frac{\partial^2}{\partial \theta^2} , \tag{2.5}$$

and $p^*$ is the reduced pressure defined by

$$p^* = p - \tfrac{1}{2}\rho\Omega^2(R + r\cos\theta)^2 . \tag{2.6}$$

As $u, v$ and $w$ are independent of $z$ in the fully developed region, it follows that

$$-\frac{\partial p^*}{\partial z} = C , \tag{2.7}$$

where $C$ is a positive constant. The boundary conditions for the velocity $u$, $v$ and $w$ are no-slip conditions on the wall of the pipe:

$$u = v = w = 0 \quad \text{at} \quad r = d/2 . \tag{2.8}$$

As all the trial computations on the whole cross-section gave symmetric solutions, we impose symmetry condition along the $x$-axis:

$$\frac{\partial u}{\partial \theta} = \frac{\partial w}{\partial \theta} = 0 \quad \text{and} \quad v = 0 \quad \text{at} \quad \theta = 0, \pi . \tag{2.9}$$

From the viewpoint of computational fluid dynamics, this flow is parabolic. The conditions for a flow to be parabolic are the existence of a predominant flow direction, negligible diffusion in that direction and negligible pressure variation in the cross-stream direction (Patankar 1980). Compared to an elliptic flow, parabolic flow can be computed with little numerical (false) diffusion. Therefore, accurate computation is possible with moderate grid density and with a modest difference scheme.

The numerical scheme employed to solve equations (2.1)–(2.4) is based on the well-established finite-volume approach (Patankar 1980). The main features of this method include a staggered mesh system, a power-law formulation for the combined convection–diffusion influence, and the well-known SIMPLE procedure for velocity–pressure linkage. The computational code is essentially the same as that used in the previous papers, and its reliability has been confirmed through the various comparisons of the computed results with reliable experimental data.

The grid density employed is 42 in the $r$-direction and 37 in the $\theta$-direction. The grid spacing is almost uniform in the $\theta$-direction, while the grid lines are more closely spaced near the wall than near the centre in the $r$-direction. The grid independence of the $42 \times 37$ grid computation was confirmed by repeating calculations with finer and coarser grids. A convergence criterion was specified with all the normalized residual errors for $u, v, w$ and mass to be less than $10^{-6}$.

## 3. Similarity consideration

To elucidate the flow characteristics, it is essential to know the dynamical similarity of the flow and to use physically appropriate parameters to represent computational or experimental results. However, there has been no such discussion in the past for the flow in rotating curved pipes, and arbitrary parameters were derived by scaling with little physical significance. For example, some authors derived parameters by scaling the cross-sectional velocities $u$, $v$ by $\nu/d$ (for example, Ito *et al.* 1987, 1988; Daskopoulos & Lenhoff 1990). Although the viscous velocity, $\nu/d$, is the velocity scale for laminar flow without secondary flow in stationary straight pipes, it no longer is the velocity scale once secondary flow occurs. It contains neither the curvature effect nor the rotation effect which cause secondary flows. Correct governing parameters can only be obtained by scaling $u$, $v$ by a velocity scale for secondary flow.

We can take either of the two limiting flows as a reference. If we take the curved pipe flow, the velocity scale of the secondary flow, $U_S$, is obtained from the balance between inertia and centrifugal forces as

$$U_S = w_m/\lambda^{1/2} . \tag{3.1}$$

The cross-sectional quantities $u, v$ and $p^*$ are scaled by $U_S$, the axial quantity $w$ by the axial velocity scale $w_m$. Thus the scaled variables are as follows:

$$\left.\begin{aligned} \tilde{u} &= \frac{u\lambda^{1/2}}{w_m} , \quad \tilde{v} = \frac{v\lambda^{1/2}}{w_m} , \quad \tilde{w} = \frac{w}{w_m} , \\ \tilde{p}^* &= \frac{p^*\lambda}{\rho w_m^2} , \quad \tilde{C} = \frac{d\lambda^{1/2}C}{\rho w_m^2} , \quad \tilde{r} = \frac{r}{d} . \end{aligned}\right\} \tag{3.2}$$

The dimensionless governing equations are then given by

$$\frac{\partial}{\partial \tilde{r}}(\tilde{r}\tilde{u}) + \frac{\partial \tilde{v}}{\partial \theta} = 0 , \tag{3.3}$$

$$\tilde{u}\frac{\partial \tilde{u}}{\partial \tilde{r}} + \frac{\tilde{v}}{\tilde{r}}\frac{\partial \tilde{u}}{\partial \theta} - \frac{\tilde{v}^2}{\tilde{r}} = -\frac{\partial \tilde{p}^*}{\partial \tilde{r}} + \tilde{w}^2\cos\theta + 2F\tilde{w}\cos\theta + \frac{1}{K_{LC}}\left(\tilde{\nabla}^2\tilde{u} - \frac{\tilde{u}}{\tilde{r}^2} - \frac{2}{\tilde{r}^2}\frac{\partial \tilde{v}}{\partial \theta}\right) , \tag{3.4}$$

$$\tilde{u}\frac{\partial \tilde{v}}{\partial \tilde{r}} + \frac{\tilde{v}}{\tilde{r}}\frac{\partial \tilde{v}}{\partial \theta} + \frac{\tilde{u}\tilde{v}}{\tilde{r}} = -\frac{1}{\tilde{r}}\frac{\partial \tilde{p}^*}{\partial \theta} - \tilde{w}^2\sin\theta - 2F\tilde{w}\sin\theta + \frac{1}{K_{LC}}\left(\tilde{\nabla}^2\tilde{v} - \frac{\tilde{v}}{\tilde{r}^2} + \frac{2}{\tilde{r}^2}\frac{\partial \tilde{u}}{\partial \theta}\right) , \tag{3.5}$$

$$\tilde{u}\frac{\partial \tilde{w}}{\partial \tilde{r}} + \frac{\tilde{v}}{\tilde{r}}\frac{\partial \tilde{w}}{\partial \theta} = \tilde{C} - \frac{2}{Ro}(\tilde{u}\cos\theta - \tilde{v}\sin\theta) + \frac{1}{K_{LC}}\tilde{\nabla}^2\tilde{w} , \tag{3.6}$$

where

$$\tilde{\nabla}^2 = \frac{1}{\tilde{r}}\frac{\partial}{\partial \tilde{r}}\left(\tilde{r}\frac{\partial}{\partial \tilde{r}}\right) + \frac{1}{\tilde{r}^2}\frac{\partial}{\partial \theta} . \tag{3.7}$$

It can be seen from the above equations that, even when the effect of $\lambda$ is negligible, laminar flows in rotating curved pipes are characterized by three parameters: the Dean number $K_{LC}$, a body force ratio $F = \lambda/Ro$ and the Rossby number $Ro$. If we take the rotating pipe flow as reference, $U_S = w_m/|Ro|^{1/2}$ and $K_{LR}$ appears instead of $K_{LC}$ together with $F^{-1}$ and $Ro$ in the flow equations. The meaning of the Dean number $K_{LC}$ is the square root of the product of (inertia force/viscous force) and (centrifugal force/viscous force). The parameter $K_{LR}$ is obtained by replacing the centrifugal force in $K_{LC}$ with the Coriolis force. We see that $K_{LC}$ appears as an inverse coefficient of the diffusion terms, just like $Re$ in standard dimensionless equations for flow without body force. Actually $K_{LC}$ or $K_{LR}$ is the Reynolds number in the cross-section, $U_S d/\nu$. Thus the flow may conveniently be

classified as viscous or boundary layer flow depending on whether $K_{LC}$ is small or large.

The body force ratio $F = \lambda/Ro$ is a new parameter, which represents the ratio of the Coriolis force to the centrifugal force. Negative values of $F$ means $\Omega < 0$, while $F = -1$ indicates that the two forces are of the same magnitude but in opposite directions. As the magnitude of $F$ is equal to $(K_{LR}/K_{LC})^2$, the change of $F$ with keeping $K_{LC}$ constant is equivalent to the change of $K_{LR}$.

The Rossby number $Ro$ represents the ratio of the inertia force to the Coriolis force. When $Ro$ is large enough, the effect of $Ro$ disappears from the flow system. The curvature parameter $\lambda$ is the ratio of the inertia force to centrifugal force. The condition that both of $\lambda$ and $Ro$ are large enough is the condition where the analogy between two limiting flows is valid. When $Ro$ is so small in magnitude that the Coriolis force dominates the axial flow field, a different flow configuration appears: the contours of axial velocity are almost parallel to the axis of rotation in the inviscid core and the location of maximum axial velocity is on the $y$-axis. It is a characteristic of the Taylor–Proudman effect where the fluid motion tends to be two-dimensional.

Here we note the another definition of the Dean number based on pressure gradient, $D = Cd^3/(\mu\nu\lambda^{1/2})$, where $C$ is given in (2.7) and $\mu$ is the viscosity. For fully developed flow in stationary curved pipes, using $K_{LC}$ or $D$ makes little difference in theoretical studies, although $D$ is difficult or impossible to use in experimental works and in developing flows. In rotating curved pipe flow, however, we have to note that $C$ depends on effects of both curvature and rotation, which reflect on the physical meaning of $D$. Therefore, $D$ is not independent of a rotation parameter. This seems to be a distinct shortcoming of using $D$ for the flow in rotating curved pipes.

## 4. Results and discussion

### 4.1. *Flow structure*

Computed flow structures for large Rossby numbers will be shown and discussed first. Curved conditions ($K_{LC}$ and $\lambda$) will be kept constant, while the rotating condition ($Ro$, thus $F$) will be changed successively while keeping $|Ro| > 8$. Examples will be given for two values of the Dean number, $K_{LC} = 100$ and 500. Dotted lines show negative streamfunctions in the contours.

Figure 2 shows computed contours of dimensionless axial velocity and secondary streamlines for the moderate value of $K_{LC} = 100$. For $F = 1$, where both the centrifugal and the Coriolis forces act radially outwards, two secondary flows in the same direction are superimposed and the resultant flow is intensified. Flow structures are then similar to those of a larger $K_{LC}$ flow in stationary curved pipes. When $F = 0$ (no rotation), only the secondary flow due to the centrifugal force exists.

In the case of negative rotation, two forces act in opposite directions and two counter-rotating vortices can coexist when the strengths of two vortices are of the same magnitude. When $F = -1.10$, a secondary flow due to the Coriolis force emerges along the inner wall of the curved pipe. As the secondary flow is in the opposite direction to that due to the centrifugal force, it weakens the effect of the latter on the axial flow. A boomerang-shaped pattern, which characterizes the $w$-contour at $F = 1.0$ and 0, now disappears and the location of the maximum axial velocity shifts toward the centre of the pipe. At $F = -1.20$ and $-1.25$, two secondary vortices of almost the same intensity but in opposite directions coexist. The effects of the two secondary flows on the primary flow neutralize each other, and a $w$-contour is, in

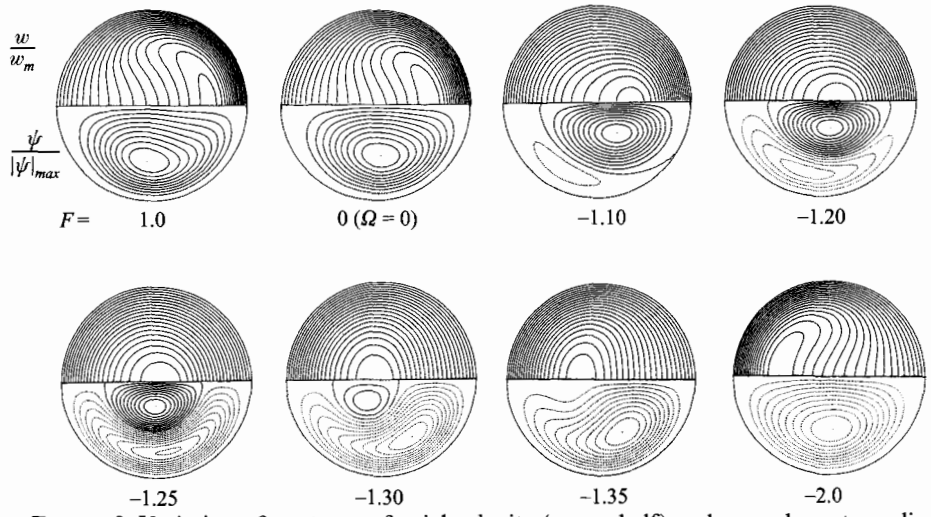


FIGURE 2. Variation of contours of axial velocity (upper-half) and secondary streamline (lower-half) with $F$ at $K_{LC} = 100$ and $\lambda = 50$.

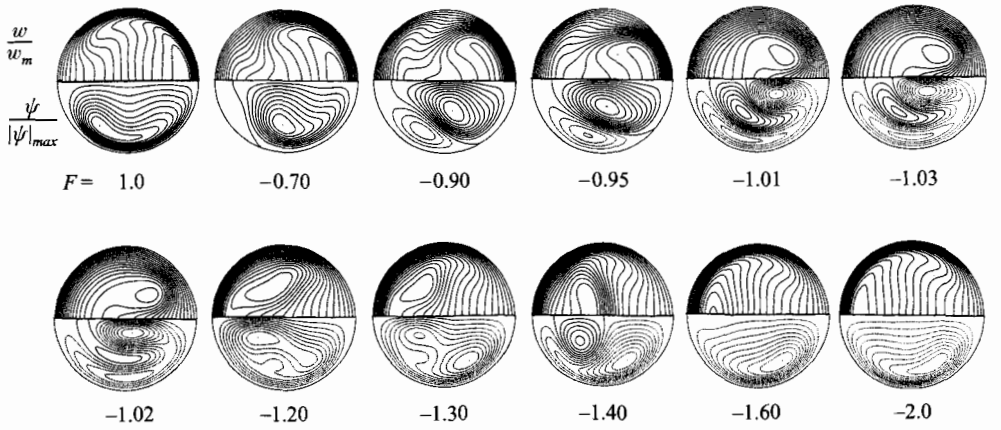


FIGURE 3. Variation of contours of axial velocity (upper-half) and secondary streamline (lower-half) with $F$ at $K_{LC} = 500$ and $\lambda = 50$.

effect, just like that of Poiseuille flow: a flow without body force. As $F$ becomes negatively larger ($F = -1.30$, $-1.35$), the secondary flow vortex, due to the centrifugal force, becomes weaker while shifting nearer to the inner bend of the pipe. Finally at $F = -2.0$, it is taken over by the secondary flow due to the Coriolis force. The contours at $F = 1.0$ are a mirror image of those at $F = -2.0$. Figure 2 gives a detailed illustration of the secondary flow reversal: how the secondary flow vortex due to the Coriolis force is generated, grows and finally replaces the other secondary flow vortex of the opposite direction due to the centrifugal force.

It is known that the curvature causes the flow on concave surfaces to be destabilized, and stationary roll cells, often called Dean vortices, occur as a result of centrifugal instability above a certain critical value of the Dean number. The occurrence of stationary roll cells in rotating curved pipes makes the flow structure even more complex. Figure 3 shows flow patterns for the higher value of $K_{LC} = 500$, in which stationary roll cells due to the centrifugal instability occur near the outer bend when $F = -1.01 \sim -1.30$.

For positive values of $F$, the situation in figure 3 is similar again to flows of larger $K_{LC}$ in stationary curved pipes. For $F = -0.70 \sim -0.95$, the secondary flow vortex due to the Coriolis force grows along the inner wall and advances to the outer wall of the curved pipe. In this case of larger $K_{LC}$, both of the secondary flows are so strong that $w$-contours appear as if they are pulled inward and outward simultaneously.

As the secondary flow due to the centrifugal force is toward the outer bend on the $x$-axis, it tends to suppress the occurrence of roll cells due to centrifugal instability on the wall at $\theta = 0°$. Development of secondary flow due to the Coriolis force nearer to the outer bend sets off the instability as a disturbance. The resulting roll cells originate near the wall at $\theta = 0°$, and the flow is directed towards the inner bend on the $x$-axis ($F = -1.01$). The location of $w_{max}$ separates into two locations. The streamlines show three vortices: two secondary flows due to the body forces and a roll cell. Secondary flow due to the Coriolis force and roll cell are combined because they have the same flow direction, while the secondary flow vortex due to the centrifugal force is isolated. The flow patterns at $F = -1.01 \sim -1.05$ are similar to the patterns in figure 11 of Daskopoulos & Lenhoff (1990), shown without physical explanations. When $F = -1.20 \sim -1.30$, a combined vortex motion of secondary flow due to the Coriolis force and the roll cell governs the flow structure in the cross-section of the pipe, while secondary flow due to the centrifugal force can barely be recognized in the streamline contours.

As the centrifugal force becomes relatively weaker, roll cells due to centrifugal instability do not occur at $F = -1.40$. The locations of $w_{max}$ then degenerate to a point, and a weak secondary flow due to the centrifugal force reappears (a similar situation to $F = -1.30$ in figure 2). Situations for $F = -1.60$ and $-2.0$ are similar to those for $F = -1.35$ and 2.0 in figure 2.

When the flow instability due to body forces takes the form of a stationary secondary flow pattern, as in the cases of Taylor and Bénard cells (see Drazin & Reid 1981) it is called the principle of exchange of stabilities. The appearance of the roll cell mentioned above is related to the Dean vortices commonly seen in a two-dimensional curved duct or rectangular curved duct above a critical Dean number. The Dean vortices in stationary curved circular pipes are not so common, but were first demonstrated in computational studies by Dennis & Ng (1982) and Nandakumar & Masliyah (1982) as one of the dual solutions of the Navier–Stokes equations. The existence of the solution in addition to the usual secondary flow pattern in stationary curved pipes was verified by flow visualization experiments (Cheng & Yuen 1984), where a four-vortex pattern (secondary flow plus roll cell) emerged on giving an artificial disturbance to the flow near the outer bend of the curved pipe. A roll cell seems to appear in curved circular pipes only when a disturbance is generated on the destabilized outer side of the pipe.

Next, we will discuss the flow structure for small Rossby number. To understand the effect of the Rossby number, the flow structure will be shown when $Ro$ is changed successively while keeping $K_{LC}$ and $F$ constant. Figure 4 shows the contours of axial velocity and secondary streamfunctions for $K_{LC} = 30$ and $F = 100$, where $Ro$ is changing in the range of $0.1 \sim 8$ while keeping $\lambda > 8$. The Taylor–Proudman effect is clearly recognized at $Ro = 0.1$; the axial iso-velocity lines are constant in the rotational vector direction in the inviscid core of the flow and secondary streamlines are symmetrical with respect to the $y$-axis. The pattern remains similar for smaller $Ro$. The structure at $Ro = 8$ is the asymptotic for large $Ro$. Contours for $Ro = 0.2 \sim 3$ show a transition between the two asymptotic situations for small and large $Ro$.

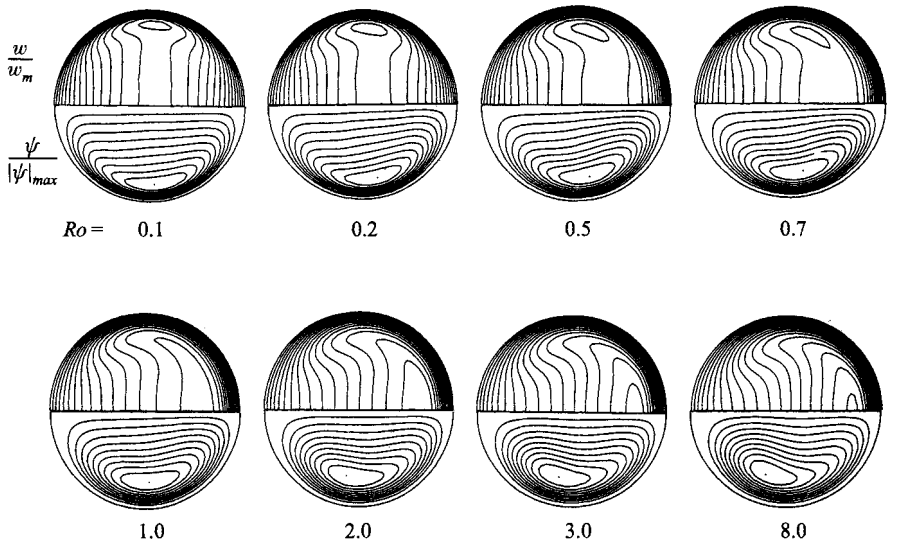


FIGURE 4. Variation of contours of axial velocity (upper-half) and secondary streamline (lower-half) with $Ro$ at $K_{LC} = 30$ and $F = 100$.

We have seen the detailed process of the secondary flow reversal around $F \approx -1$, where two body forces of opposite direction compete. For estimating the secondary flow reversal, Daskopoulos & Lenhoff (1990) gave the different criterion $D/Ta \approx -4$. In their criterion, $Ta$ varies with effects of both curvature and rotation, as does $D$ as mentioned in §3. Therefore, the ratio $D/Ta$ seems to be impossible to understand and manage. The reversal should be controlled by the balance between two body forces. From figures 2, 3 and 5 shown later, and from the meaning of the dimensionless numbers, $F \approx -1$ seems to be the obvious criterion.

### 4.2. *Friction factor*

The friction factor is the most important flow property in engineering applications. Extensive and precise measurements on pressure loss were made by Ito *et al.* (1987, 1988) for constant $K_{LC}$ and for constant $R_\Omega$ points, the total number of the tabulated data being over 550. These data will be used for comparison and validation of the present study.

First, we show the friction factor for $\lambda, |Ro| > 8$. To have an overall view of behaviour of the friction factor for large $|Ro|$, figure 5 shows the computed values of the Fanning friction-factor ratio $f/f_0$ together with the data for constant-$K_{LC}$ experiments, where $f = \bar{\tau}_w/\frac{1}{2}\rho w_m^2$ in which $\bar{\tau}_w$ is the peripheral average of wall friction and $f_0 = 16/Re$ is the non-rotating straight pipe value. All curves have their minimum around $F \approx -1.0$ where secondary flow reversal occurs. Steady solutions cannot be obtained for a certain range of $F \approx 1$ (the solid lines break there in figure 5) for $K_{LC} = 707$ and 1414. The roll cells due to flow instability do not occur in the lower two cases, $K_{LC} = 141.4$ and 282.8. The computational results agree well with the experimental data, including minimum values. A similar comparison for constant-$R_\Omega$ cases also showed good agreement.

The computed results are shown in figure 6(*a,b*) for a wide range of $K_{LC}$ while keeping $F$ constant for positive and negative rotation. The dotted lines in the figure show the friction formula for $F = 0$, non-rotating curved pipe flow. For positive rotation, $f$-curves increase in almost a parallel manner from the non-rotating flow

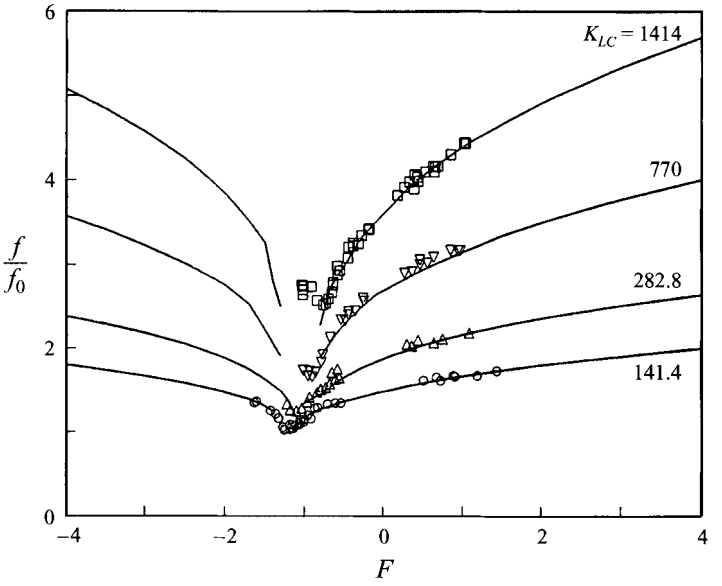


FIGURE 5. Friction factor ratio at constant Dean number: ———, present computation ($\lambda = 50$); ○, △, ▽, □, experimental data by Ito *et al.* (1987).

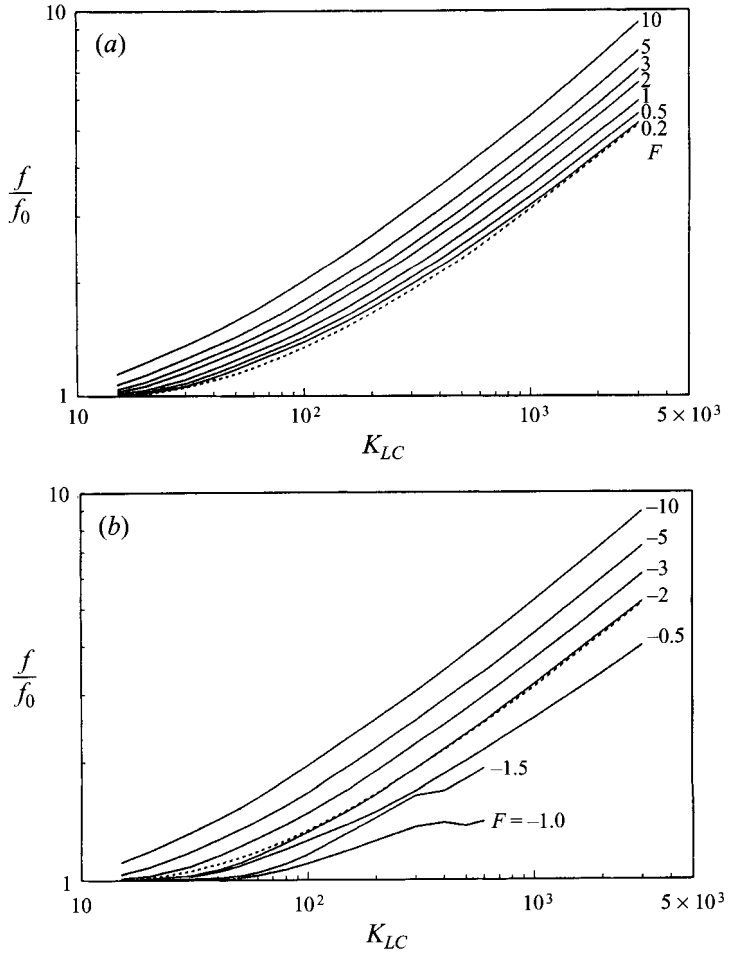


FIGURE 6. Variation of computed friction factor ratio with the Dean number: ———, present computation ($\lambda = 50$); - - - -, curve for $F = 0$ equation (4.1*a*). (*a*) Positive rotation; (*b*) negative rotation.

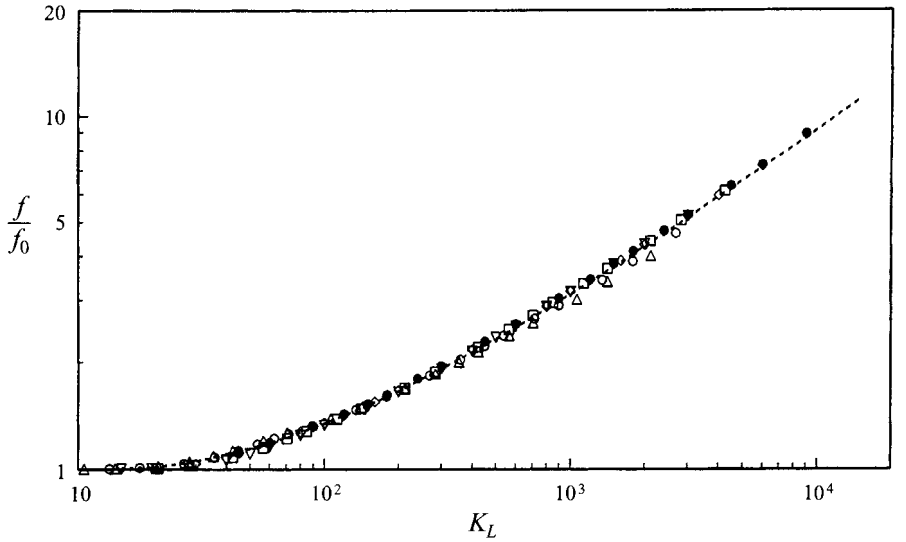


FIGURE 7. Comparison of the friction formula ( 4.1*a*,*b*) with the computed values for negative rotation: - - - -, (4.1*a*,*b*); computed values ($\lambda = 50$) ○, $F = -0.2$; △, $-0.5$; ▽, $-2$; □, $-3$; ◇, $-5$; ●, $-10$.

curve as $F$ increases. For negative rotation, $f$-curves first decrease, taking a minimum at $F \approx -1$, then increase as $F$ increases negatively. Numerical computations for $F = -1.0$ and $-1.5$ become unstable for large values of $K_{LC}$ and steady solutions cannot be obtained. The curve for $F = -2$ nearly coincides with that for $F = 0$ for the entire range of $K_{LC}$, which suggests that the $f$-curves in figure 6 are approximately symmetrical with respect to $F = -1.0$.

In the previous paper (Ishigaki 1994), an analogy formula for the friction factor common to both fully developed laminar flows in non-rotating curved pipes and in rotating straight pipes was given as follows:

$$\frac{f}{f_0} = 0.0899 K_L^{1/2}(1 + 12.4 K_L^{-0.701}) , \tag{4.1a}$$

for $K_L < 3000$, and $\lambda, Ro > 8$. When the right-hand side of (4.1*a*) yields a value below 1, $f/f_0$ should be set to 1. In the formula $K_L$ represents $K_{LC}$ for non-rotating curved pipe flow and $K_{LR}$ for rotating straight pipe flow. It is the formula for $F = 0$, that has been used in figure 6 as the dotted curve. If $K_{LC}$ is replaced by $K_{LR}$, it is also an asymptotic formula for $F = \pm\infty$.

Taking it into consideration that the $f$-curves in figures 5 and 6 are approximately symmetrical with respect to $F = -1$, we try to extend (4.1*a*) to rotating curved pipe flow by making the transformations $K_L = K_{LC}(F + 1)^{1/2}$ for $F > -1$ and $K_L = K_{LC}(|F| - 1)^{1/2}$ for $F < -1$. The transformations embody their limiting forms: $K_L \to K_{LC}$ as $F \to 0$ and $K_L \to K_{LR} = Re/|Ro|^{1/2}$ as $F \to \pm\infty$. Figure 7 shows that computational results, except for those of $F = -1$ and $-1.5$, lie on (4.1*a*) for negative rotation. A similar comparison for positive rotation showed better agreement.

The corresponding comparisons of (4.1*a*) with experimental data are shown in figures 8(*a*) and 8(*b*), which include all the experimental data by Ito *et al.* (1987, 1988) for $\lambda, |Ro| > 8$ except for $-0.80 > F > -1.30$. If the excluded range of $F$ is taken narrower, the scatter of the data abruptly increases. Thus, based on the comparison with the experimental data, the applicable range of the transformation is specified as

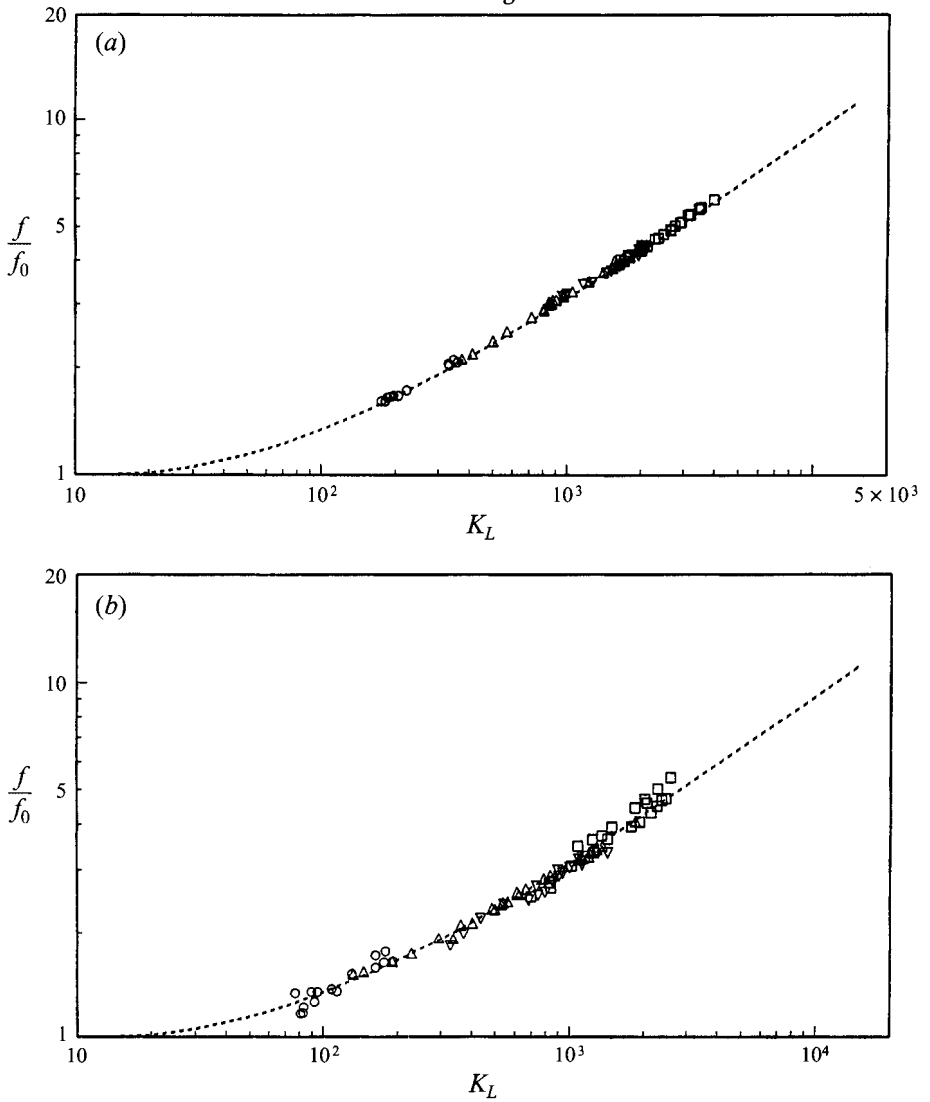


FIGURE 8. Comparison of the friction formula (4.1*a*,*b*) with experimental data for $|Ro| > 8$: - - - -, (4.1*a*,*b*); experimental data by Ito *et al.* (1987, 1988) ○, $\lambda = 26.8$; △, 10.0; ▽, 8.3; □, 8.25. (*a*) Positive rotation; (*b*) negative rotation.

follows:

$$\left.\begin{aligned} K_L &= K_{LC}(F+1)^{1/2} \quad \text{for} \quad F > -0.80, \\ K_L &= K_{LC}(|F|-1)^{1/2} \quad \text{for} \quad F < -1.30. \end{aligned}\right\} \tag{4.1b}$$

The composite parameter $K_L$ can be regarded as a convenient governing parameter for the flow. As it is not derived from the basic equations, it is not an exact one but of approximate nature.

Next, we discuss the friction factor for a small value of $|Ro|$, but still $\lambda > 8$. The friction factor increases as $Ro$ becomes smaller. Figure 9 shows computed results for $|Ro| = 0.5$, together with (4.1*a*,*b*) and experimental data. Three computed results with different flow dimensions but of the same $|Ro|$ fall onto a single curve, indicating that the choice of parameters, as well as $K_L$ as a governing parameter, is consistent

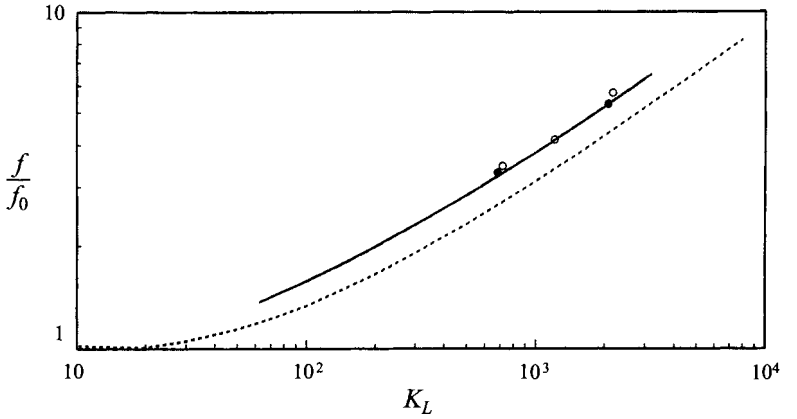


FIGURE 9. Friction factor ratio at $|Ro| = 0.5$. Computation results: ———, $Ro = 0.5$, $\lambda = 20$; —·—·—, $Ro = -0.5$, $\lambda = 20$; —··—··—, $Ro = 0.5$, $\lambda = 50$ (indistinguishable). Experimental data by Ito *et al.* ○, $0.45 < Ro < 0.55$; ●, $-0.45 > Ro > -0.55$. - - - -, (4.1*a*,*b*).

with the dynamical similarity of the flow. The computed results agree well with experimental data for $|Ro| \approx 0.5$.

Computational results for $0.1 < |Ro| < 8$ are approximated well by (4.1*a*,*b*) multiplied by the following function:

$$\zeta = 1 + 0.047 K_L^{0.156} |Ro|^{-0.721}. \tag{4.1c}$$

Figure 10 shows the comparison between (4.1*a*,*b*,*c*) and the experimental data for three regions of $|Ro|$. Figures 8 and 10 contain all the experimental data by Ito *et al.* (1987, 1988) except for $-0.8 > F > -1.3$. The agreement between the proposed semi-empirical formula and the experimental data is very good. The effect of $Ro$ on the friction factor can be estimated from (4.1*c*) to be $\zeta = 1.14$ for $Ro = 1$, 1.23 for $Ro = 0.5$ and 1.73 for $Ro = 0.1$, when $K_L = 10^3$. The effect of $Ro$ on the friction factor is smaller than 5% when $|Ro| \gtrsim 4$, from the condition $\zeta < 1.05$.

### 4.3. *Secondary flow properties*

Although $U_S$ in (3.1) was employed in deriving the similarity parameters, $U_S$ is in fact the secondary velocity scale for stationary curved pipe flow. As the composite parameter $K_L$ in ( 4.1*b*) should have the meaning of the cross-sectional Reynolds number, the cross-sectional velocity scale for rotating curved pipe flow may be assumed to be $K_L \nu/d$. This velocity scale contains effects of both curvature and rotation. Excluding the singular region of $F$ in (4.1*b*), this scale should be used for normalizing secondary flow properties.

As an example of a secondary flow property, we will take its intensity. The secondary stream function $\psi$ takes its extremum at the centre of the secondary flow vortices. Figure 11 shows the variation of its absolute maximum, $|\psi|_{max}$, with $K_L$ for $\lambda$, $|Ro| > 8$, where the dotted line shows that of a non-rotating curved pipe flow ($F = 0$). The computed curves show quite similar behaviours. The secondary flow becomes weaker as $|Ro|$ decreases (see Ishigaki 1996*b*). Additional flow properties, such as the axial velocity maximum, can be seen in Ishigaki (1993, 1996*b*).

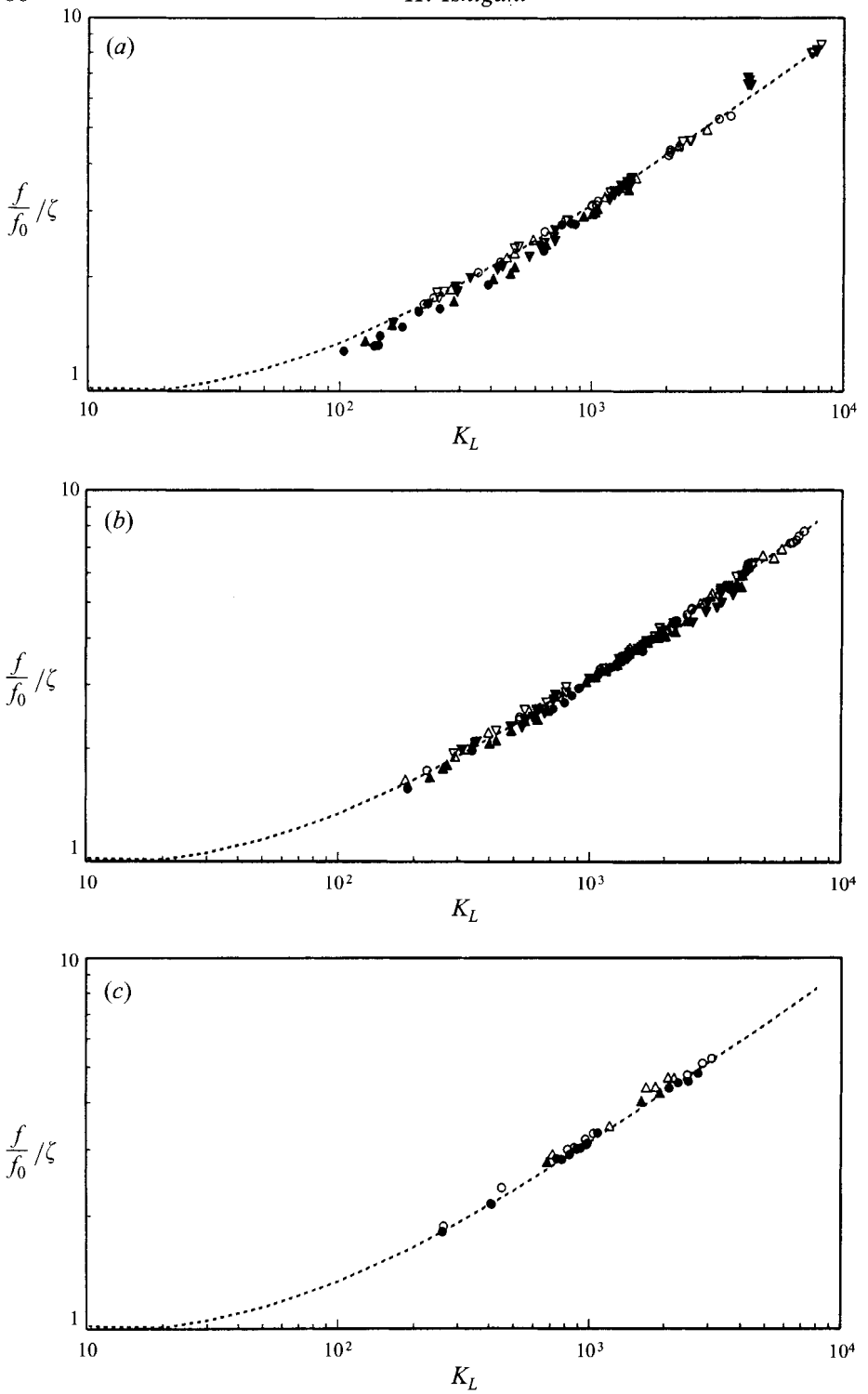


FIGURE 10. Comparison of the correction formula (4.1*c*) with experimental data for three regions of $|Ro|$: - - - -, (4.1*a*,*b*,*c*). (*a*) $8 > |Ro| > 4$. Experimental data ○, $8 > Ro > 6$; △, $6 > Ro > 5$; ▽, $5 > Ro > 4$; ●, $-8 < Ro < -6$; ▲, $-6 < Ro < -5$; ▼, $-5 < Ro < -4$. (*b*) $4 > |Ro| > 1$. Experimental data ○, $4 > Ro > 3$; △, $3 > Ro > 2$; ▽, $2 > Ro > 1$; ●, $-4 < Ro < -3$; ▲, $-3 < Ro < -2$; ▼, $-2 < Ro < -1$. (*c*) $1 > |Ro| > 0$. Experimental data ○, $1 > Ro > 0.5$; △, $0.5 > Ro > 0$; ●, $-1 < Ro < -0.5$; ▲, $-0.5 < Ro < 0$.

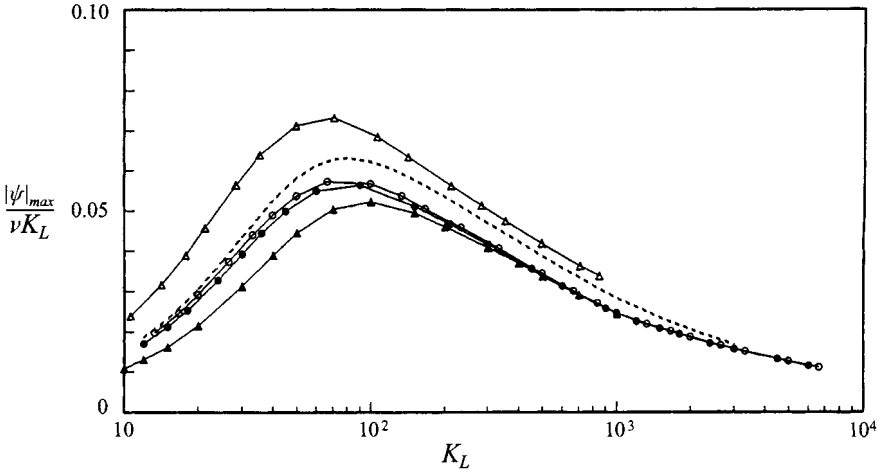


FIGURE 11. Variation of stream function extremum $|\psi|_{max}$ with $K_L$ at large $|Ro|$ ($\lambda$, $|Ro| > 8$): - - - -, $F$=0; —○—, 10; -△-, -0.5; -▲-, -2; —●—, -10.

## 5. Conclusions

Fully developed laminar flows in rotating curved pipes have been studied for both positive and negative rotations. Similarity considerations revealed that the general flow situation was governed by four parameters: the Dean number $K_{LC}$, the body force ratio $F$, the curvature parameter $\lambda$ and the Rossby number $Ro$. Computational results were given for the case when the effect of $\lambda$ on the flow characteristics was negligible. Variations of flow structures with the parameters were shown, particularly complicated structure with secondary flow reversal around $F \approx -1$ being studied in detail. Through investigating computational results and experimental data for the friction factor, a convenient governing parameter $K_L$ was suggested for correlating the flow characteristics. By using $K_L$, a semi-empirical formula for the friction factor was proposed, which showed good agreement with experimental data for a wide range of $K_{LC}$, $F$ and $Ro$. The corresponding convective heat transfer problem in rotating curved pipes has been studied elsewhere (Ishigaki 1995).

## REFERENCES

CHENG, K. C. & YUEN, F. P. 1984 Flow visualization studies on secondary flow patterns in curved tubes and isothermally heated horizontal tubes. *ASME Paper* 84-HT-62.

DASKOPOULOS, P. & LENHOFF, A. M. 1990 Flow in curved ducts. Part 2. Rotating ducts. *J. Fluid Mech.* **217**, 575–593.

DENNIS, S. C. R. & NG, M. 1982 Dual solutions for steady laminar flow through a curved tube. *Q. J. Mech. Appl. Maths* **35**, 305–324.

DRAZIN, P. G. & REID, W. H. 1981 *Hydrodynamic Stability*, p. 108. Cambridge University Press.

EUTENEUER, G. A. & PIESCHE, M. 1978 Druckabfallmessungen in stationkär rotierenden, gekrümmten Kanalstrecken mit quadratichem sowie kreisförmigen Druchflussquerchnitt. *Forsch. Ing.-wes.* **44**, 53–56.

GREENSPAN, H. P. 1968 *The Theory of Rotating Fluids*. Cambridge University Press.

HOPFINGER, E. J. 1992 *Rotating Fluids in Geophysical and Industrial Applications*, P. 3. Springer.

ISHIGAKI, H. 1993 Fundamental characteristics of laminar flows in a rotating curved pipe. *Trans. JSME* **59-561-B**, 1494–1501 (in Japanese).

ISHIGAKI, H. 1994 Analogy between laminar flows in curved pipes and orthogonally rotating pipes. *J. Fluid Mech.* **268**, 133–145.

ISHIGAKI, H. 1995 Laminar convective heat transfer in rotating curved pipes. *Trans. JSME* **61-582-B**, 672–678 (in Japanese).

ISHIGAKI, H. 1996*a* Analogy between turbulent flows in curved pipes and orthogonally rotating pipes. *J. Fluid Mech.* **307**, 1–10.

ISHIGAKI, H. 1996*b* The effect of Rossby number on flow and heat transfer in rotating curved pipes. *Trans. JSME*, **62-597-B**, 1788–1794 (in Japanese).

ITO, H., AKITA, H., HASEGAWA, S. & SUZUKI, M. 1988 Numerical and experimental study on laminar flow in a rotating curved pipe (2. constant rotational Reynolds number). *Mem. Inst. High Speed Mech.* **59**, 45–96 (in Japanese).

ITO, H., KOMAKI, H., HASEGAWA, S. & SUZUKI, M. 1987 Numerical and experimental study on laminar flow in a rotating curved pipe (1. constant Dean number). *Mem. Inst. High Speed Mech.* **58**, 185–235 (in Japanese).

ITO, H. & MOTAI, T. 1974 Secondary flow in a rotating curved pipe. *Rep. Inst. High Speed Mech.* **29**, 33–57.

LUDWIEG, H. 1951 Die ausgebildete Kanalstömung in einem rotierenden System. *Ing. Arch.* **19**, 296–308.

MATSSON, O. J. E. 1993 Time-dependent instabilities in curved rotating channel flow. *Phys. Fluids* A **5**, 1514–1516.

MATSSON, O. J. E. & ALFREDSSON, P. H. 1990 Curvature- and rotation-induced instabilities channel flow. *J. Fluid Mech.* **210**, 537–563.

MATSSON, O. J. E. & ALFREDSSON, P. H. 1994 The effect of spanwise system rotation on Dean vortices. *J. Fluid Mech.* **274**, 243–265.

MIYAZAKI, H. 1971 Combined free and forced convective heat transfer and fluid flow in a rotating curved circular tube. *Intl J. Heat Mass Transfer* **14**, 1295–1309.

MIYAZAKI, H. 1973 Combined free and forced convective heat transfer and fluid flow in a rotating curved rectangular tube. *Trans. ASME* C: *J. Heat Transfer* **95**, 64–71.

NANDAKUMAR, K. AND MASLIYAH, J. H. 1982 Bifurcation in steady laminar flow through curved tubes. *J. Fluid Mech.* **119**, 475–490.

PATANKAR, S. V. 1980 *Numerical Heat Transfer and Fluid Flow*. Hemisphere.

PIESCHE, M. 1982 Experimente zum Strömungswiderstand in genkrümmten, rotierenden Kanälen mit quadratischem Querchnitt. *Acta. Mech.* **42**, 145–151.

PIESCHE, M. & FELSCH, K. O. 1980 Experimental investigation of pressure loss in rotating curved rectangular channels. *Arch. Mech.* **32**, 747–756.

SELMI, M., NANDAKUMAR, K. & FINLAY, W. H. 1994 A bifurcation study of viscous flow through a rotating curved duct. *J. Fluid Mech.* **262**, 353–375.